Journal of Corrosion and Materials
www.corromat.com

J. Corros. Mater. (2026) 5(2), 151–162.

Electrochemical Protection of AZ31B Magnesium Alloy by Zinc-Phosphate Nanoflower Sealed MAO Coatings in Chloride and Acidic Sulfate Media

Gil Anderi da Silva[1,*]

Department of Chemical Engineering, University of São Paulo, São Paulo–SP 05508-010, Brazil

*Corresponding author: ganderis@usp.br

(Received: 7 July 2026. Received in revised form: 9 September 2026. Accepted: 23 September 2026. Published online: 30 December 2026.)

Abstract

The AZ31B magnesium alloy has a low density, appreciable strength, and engineering deformability; however, the alloy's resistance to aqueous corrosion is compromised by fast anodic dissolution, hydrogen gas evolution, and poor formation of stable passive film. The process of micro-arc oxidation creates a protective coating with a ceramic structure, which enhances corrosion resistance, while pores and microcracks are still available for contact with highly-chlorinated and acidic electrolytes. The performance of three AZ31B magnesium alloy surfaces under consideration: unmodified AZ31B alloy (AZ31B); micro-arc oxidation modified AZ31B (AMAO); and zinc-phosphate nanoflowers with a hydrophobic surface treatment on the basis of micro-arc oxidation coating (AMAO@P-ZPNF), will be analyzed in terms of corrosion potential, corrosion current density, coating resistance, charge transfer resistance, anti-corrosive efficiency, acid retention, and dual-environment barrier score in 3.5 wt% NaCl and 0.5 mol L^{-1} H_2SO_4. In 3.5 wt% NaCl, the corrosion current densities decrease from 4.862×10^{-5} A cm^{-2} (AZ31B) to 1.478×10^{-6} A cm^{-2} (AMAO) to 3.775×10^{-8} A cm^{-2} (AMAO@P-ZPNF). The values for the same conditions in 0.5 mol L^{-1} H_2SO_4 are 2.747×10^{-4} A cm^{-2}, 8.029×10^{-6} A cm^{-2}, and 9.497×10^{-8} A cm^{-2}. The charge-transfer resistance in 3.5 wt% NaCl increases to 3.517×10^{6} Ω cm^2. For the acid solution, the corresponding value is 2.534×10^{6} Ω cm^2. The dual-environment barrier score in the case of AMAO@P-ZPNF is 1.067×10^{4}. The value of the score for the AMAO coating is 82.58, while for the uncoated AZ31B alloy, it is 1. It was demonstrated that the additional treatment with zinc phosphate nanoflowers increases the anti-corrosive protection level due to sealed pore openings, decreased conductivity of the electrolyte, increased diffusion pathways, and maintained strong resistance to the charge transfer across the interface.

Keywords: AZ31B magnesium alloy; micro-arc oxidation; zinc phosphate nanoflowers; superhydrophobic coating; electrochemical impedance spectroscopy; corrosion current density; acidic sulfate corrosion.

1. Introduction

The significance of magnesium alloys as light-weighting material in transportation, electronic devices, aviation parts, and biocompatible medical equipment is evident due to their combination of low weight, relatively good specific strength, machining, dampening abilities, and recyclability. In applications where weight reduction is critical, Mg-Al-Zn alloy known as AZ31B represents another desirable candidate. However, the usage of such a material has been impeded by its elevated electrochemical reactivity and insufficient ability to create a passive film when exposed to water-based environments. Thin and easily disturbed chemically unstable oxide and hydroxide layers of magnesium become the weak point when any aggressive media gain access to the underlying metal. Thus, magnesium anode oxidation and hydrogen evolution take place in cathode spots with formation of porous corrosion products, which fail to produce a stable passive film [1]. Recent magnesium-corrosion reviews confirm that this chemical activity remains a major limitation for service deployment [2]. Earlier surveys of magnesium-alloy corrosion likewise emphasize the instability of the natural oxide/hydroxide surface in aggressive environments [3]. For biomedical magnesium, this same reactivity becomes useful only when degradation can be carefully controlled [4].

The influence of solution composition on AZ31B corrosion processes is obvious. Chlorine-containing solutions increase solubility of $Mg(OH)_2$ and favor formation of soluble compounds of magnesium and their further participation in chemical reactions. At that, active areas of the surface will be renewed constantly. Additionally, acidified solutions are even more severe since acid ions are able to dissolve oxide/hydroxide layers instantly and accelerate the metal removal. Marine aerosols, deicing agents, acidic atmospheres, and various wetting/drying conditions might result in alternating corrosive effects related to ion migration and direct dissolving of the substrate. Therefore, protective coatings should not only decrease electrolyte penetration but also ensure stability of coating and non-participation in Faraday reactions. Critical reviews of protective coatings show that magnesium-alloy protection requires both barrier function and chemical stability [5]. Conversion-coating studies further confirm that surface chemistry is central to corrosion resistance on magnesium alloys [6]. Biomedical-coating research adds that coating chemistry must also remain compatible with the intended service environment [7].

One of the effective approaches for magnesium alloys treatment is micro-arc oxidation also named plasma electrolytic oxidation. With its help, a ceramic-like oxide layer can be formed on the external surface of the substrate due to the action of electric high voltage discharge. Plasma electrolysis provides the general surface-engineering basis for forming such oxide layers [8]. Micro-arc oxidation studies on magnesium alloys show that alkaline silicate electrolytes can produce ceramic-like coatings with characteristic discharge structures [9]. Phosphate PEO coatings demonstrate that corrosion resistance depends strongly on the formed oxide structure and chemistry [10]. Broader PEO reviews also describe the method as a useful route for producing anodized coatings on lightweight metals [11]. The layer obtained through this technology may provide enhanced mechanical characteristics and corrosion resistance while keeping its shape unchanged. On the other hand, the process of oxide generation itself has certain limitations in form of defect formation such as discharge pores, micro-cracking, nodular structure of oxide, and, finally, connected cracks through which electrolyte migration is possible.

Sealing of the MAO coating is required under severe corrosion environments. A wide range of approaches has been applied to minimize the accessibility of open defects: sealants, sol–gel layers, organic topcoats, inhibitor-containing coatings, conversion films, and hydrophobic modification of the surface. Superhydrophobic modification of the surface is particularly applicable since the combination of increased roughness and low surface energy reduces the real area of interaction between liquid and solid phases. The Wenzel model explains how roughness can modify wetting on solid surfaces [12]. The Cassie–Baxter description further shows how trapped air can reduce liquid–solid contact on textured surfaces [13]. Modern wetting analysis confirms that roughness and surface chemistry jointly determine hydrophobic behavior [14]. On magnesium alloy surfaces, a superhydrophobic state can hinder the formation of continuous ionic channels, reduce the residence time of electrolyte inside defects, and diminish corrosion current density. Superhydrophobic light-alloy surfaces have been shown to improve corrosion protection through reduced electrolyte contact [15]. Micro-arc-oxidized Mg-Li-Ca alloy coatings also demonstrate the corrosion benefit of superhydrophobic modification [16]. Reviews of superhydrophobic corrosion-protection surfaces confirm the same barrier principle across several material systems [17].

The superhydrophobicity per se is insufficient for effective corrosion protection. The roughness can be destroyed, the chemistry capable of low surface energy can deteriorate, and the electrolyte can eventually penetrate into the pores if the underlying surface coating remains permeable. For a robust surface, one needs to create a stable oxide film as a base; an external coating hindering the formation of discharge pores; chemical resistance to aggressive ions; and high charge-transfer resistance of active interfaces. Conducting-polymer studies on active metals show that additional functional layers may modify interfacial protection [18]. Organofunctional silanes also provide corrosion protection by improving the connection between inorganic surfaces and outer organic layers [19]. Robust slippery coatings on AZ31B further show that surface architecture and chemical compatibility can jointly increase corrosion resistance [20]. Nanoflowers of zinc phosphate have all those properties due to microclusters and nanopetals providing increased roughness, promoting air entrapping during hydrophobic modification, and possessing sparingly soluble phosphate phase. The zinc phosphate nanoflowers deposited onto the MAO surface will help to shield pore openings, increase the path length for ion transport, and diminish the likelihood that chloride or acid gets to the AZ31B matrix.

The electrochemical polarization and EIS techniques are useful in evaluating the performance of multi-layered coatings. Corrosion current density i_{corr} quantifies the instant corrosion activity of the system, whereas E_{corr} characterizes the potential of mixed reactions between anodic and cathodic sites. The Stern–Geary relation provides the classical polarization basis for connecting corrosion current with corrosion kinetics [21]. The data from impedance spectra include coating resistance R_c, charge-transfer resistance R_{ct}, capacitive effects, and solution resistance. Electrochemical impedance spectroscopy is useful for investigating corrosion-protection methods because it separates solution, coating, and interface contributions [22]. Impedance-spectroscopy theory also supports interpretation of dispersive capacitive behavior in complex electrochemical systems [23]. Recent impedance tutorials clarify the practical meaning of equivalent-circuit elements and fitting parameters [24]. For a coated magnesium alloy, high values of R_c reflect limited penetration of electrolyte, whereas large R_{ct} indicate reduced interfacial Faradaic reaction rate.

This work considers AZ31B, AMAO, and AMAO@P-ZPNF samples exposed to neutral chloride and acidic sulfate solutions. The main aim is to assess the effect of nanoflower sealing on the corrosion current suppression, coating resistance, charge transfer resistance, and acid penetration. It should be noted that the results interpretation is always tied to particular measurable parameters and the corresponding surface features: an uncoated AZ31B with natural film, AMAO sample with a porous ceramic-like oxide film, and AMAO@P-ZPNF with a nanoflower-modified surface.

2. Materials and electrochemical evaluation

The material system is based on AZ31B magnesium alloy in three different surface states. First, the uncoated AZ31B reveals the natural surface film of the alloy and its oxide/hydroxide coating to the corrosive medium. Second, in AMAO,

the surface of the alloy gets covered with oxide films and discharge pores generated by micro-arc oxidation. Third, the AMAO@P-ZPNF state implies deposition of zinc phosphate nanoflower arrays and subsequent hydrophobic modification. These three surface states reflect the transition from the naturally chemically fragile oxide coating to the porous one and further modification with the nanoflowers [25].

The electrolyte group includes 3.5 wt% NaCl and 0.5 mol L^{-1} H_2SO_4 solutions. Chloride solution acts to increase magnesium hydroxide instability and cause localized corrosion. The sulfuric acid solution increases oxidation/hydrolysis rate and hydrogen-ion attack of the surface. The choice of both electrolytes enables evaluation of a particular surface condition under two different corrosive threats.

The protection efficiency of the coatings in terms of corrosion current reduction is estimated using

$$\eta_i = \left(1 - \frac{i_{\mathrm{corr},i}}{i_{\mathrm{corr},AZ31B}}\right) \times 100, \tag{1}$$

where $i_{\mathrm{corr},i}$ is the corrosion current density of AMAO or AMAO@P-ZPNF and $i_{\mathrm{corr},AZ31B}$ is the corrosion current density of the uncoated AZ31B in the same electrolyte. This ratio reflects the influence of a coating compared to the bare surface for a particular solution.

The resistance amplification of charge-transfer processes is evaluated using

$$A_{R_{ct}} = \frac{R_{ct,i}}{R_{ct,AZ31B}}, \tag{2}$$

where $R_{ct,i}$ and $R_{ct,AZ31B}$ are the values of charge-transfer resistance. High values of $A_{R_{ct}}$ indicate good suppression of corrosion reactions on the surface.

The dual-environment barrier score is defined as

$$\Phi = \left[\left(\frac{i^{NaCl}_{\mathrm{corr},AZ31B}}{i^{NaCl}_{\mathrm{corr},i}}\right)\left(\frac{i^{acid}_{\mathrm{corr},AZ31B}}{i^{acid}_{\mathrm{corr},i}}\right)\left(\frac{R^{NaCl}_{ct,i}}{R^{NaCl}_{ct,AZ31B}}\right)\left(\frac{R^{acid}_{ct,i}}{R^{acid}_{ct,AZ31B}}\right)\right]^{1/4}. \tag{3}$$

A higher geometric mean will reward the balance between NaCl and H_2SO_4 media. This will be achieved by reducing the corrosion current while maximizing the charge transfer resistance for both media. The acid retention factor is derived using

$$\Gamma_{acid} = \frac{R^{acid}_{ct,i}/R^{acid}_{ct,AZ31B}}{R^{NaCl}_{ct,i}/R^{NaCl}_{ct,AZ31B}}, \tag{4}$$

where the ratio of relative charge transfer benefits in acid is compared to the respective benefit in the chloride solution. If the ratio exceeds unity, it indicates that the acid retains a better relative electrochemical advantage due to the coating.

3. Results and discussion

3.1 Surface properties and coating integrity

The unprotected AZ31B surface depends upon the native film which offers little resistance once the ions (chloride or hydrogen ions) attack the metal. The typical surface shown in Figure 1 appears as a relatively smooth alloy surface with minor polishing marks and some isolated surface irregularities. This suggests the possibility of direct electrolyte contact, since there is no significant protective layer between the solution and the alloy. This kind of surface has the capability of initiating corrosion quickly upon destabilization of $Mg(OH)_2$ in chloride or dissolution in acid.

The micro-arc oxidized coating shown in Figure 2 exhibits the typical appearance of a rough ceramic coating due to the plasma-assisted growth process. Discharge pores, oxide islands and crack-like structures can be seen on the coating surface. The above-mentioned characteristics account for the dual purpose of the AMAO coating. It is an oxide layer that ensures an increased distance between the electrolyte and the substrate, but at the same time it can retain the solution at the local level and facilitate its diffusion toward the inner coating. The coating therefore improves corrosion resistance but does not behave as a completely impermeable layer.

This is because the AMAO@P-ZPNF structure in Figure 3 features dense arrays of zinc phosphate nanoflowers, which constitute a hierarchical roughness structure on the outer side of the MAO film. Such structure makes it hard for the electrolyte to enter discharge pores, resulting in hydrophobic wetting after the surface treatment. From this figure, we can see that there is a reason why the final coating influences electrolyte penetration and interfacial reaction rate.

From Figure 4, the layered structure nature of the coating known as AMAO@P-ZPNF is observed. First, there is a lower portion of AZ31B substrate, then the layer of porous oxide referred to as MAO and lastly the zinc phosphate nanoflower layer, which is on the outside. These layers are significant because they play a crucial role in the function of the coating, in that they do not protect the substrate by just one aspect. It gives adherence and ceramic strength from the MAO, while the phosphate coating makes tortuous entry into the pores difficult.

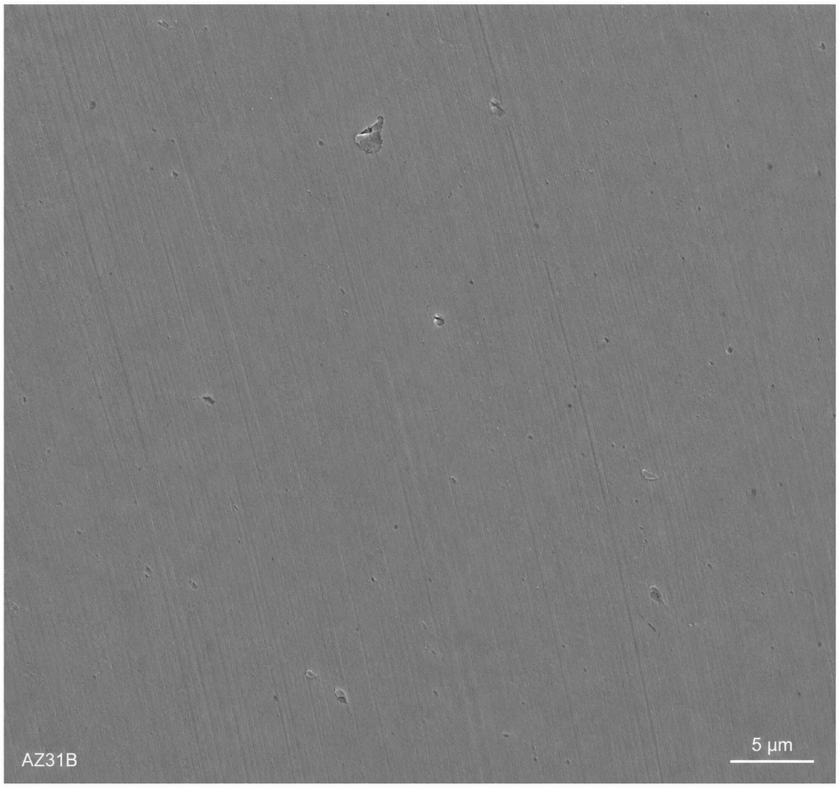

Figure 1: Bare AZ31B surface.

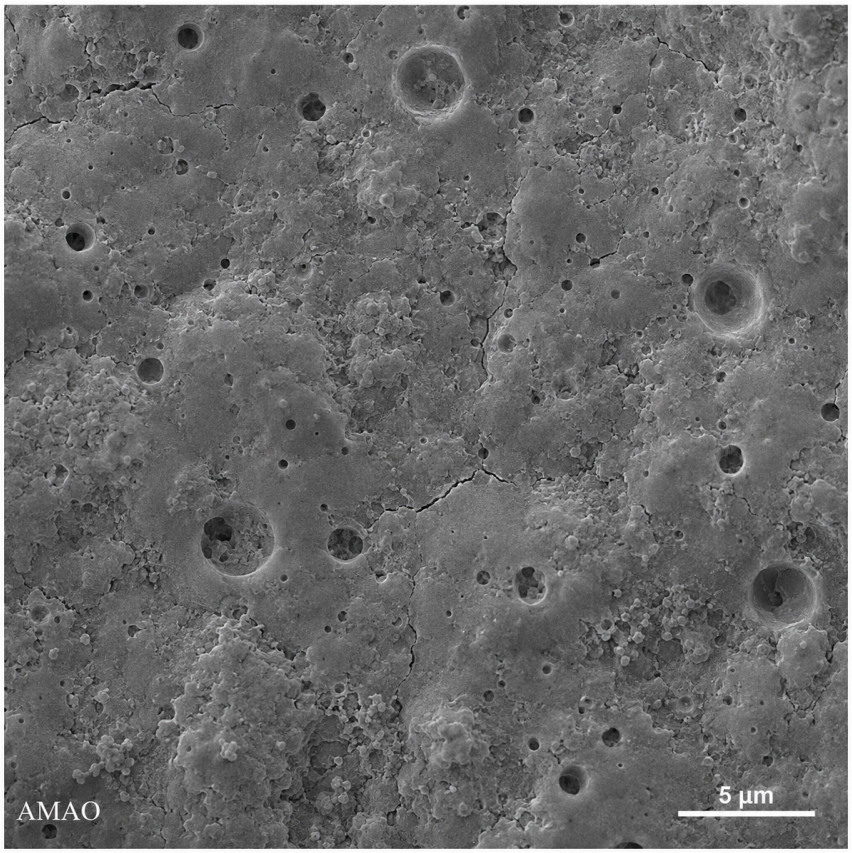

Figure 2: Porous AMAO surface.

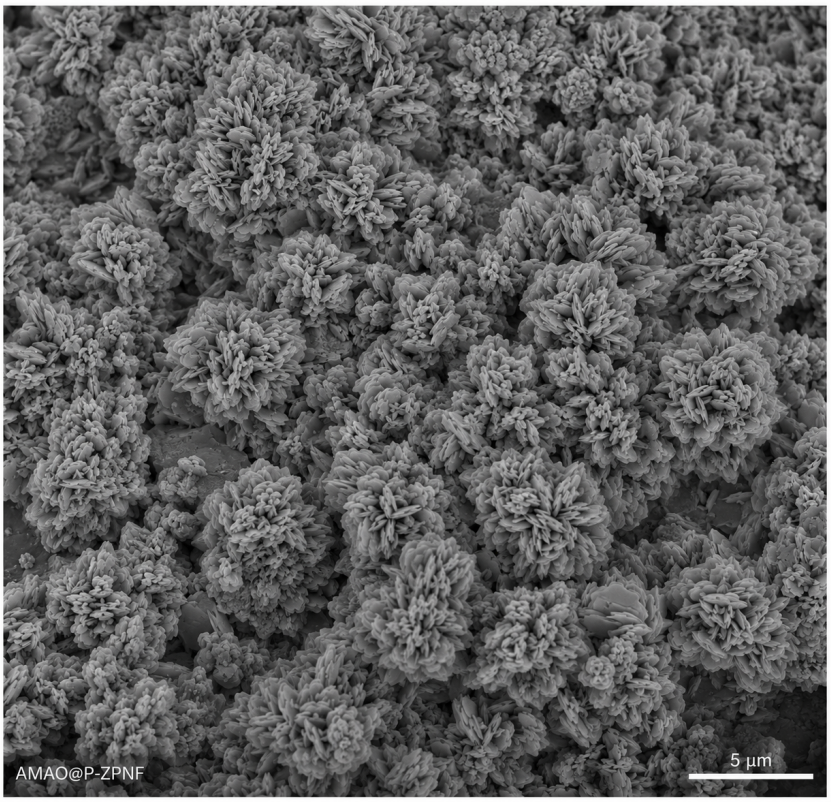

Figure 3: Nanoflower-sealed AMAO surface.

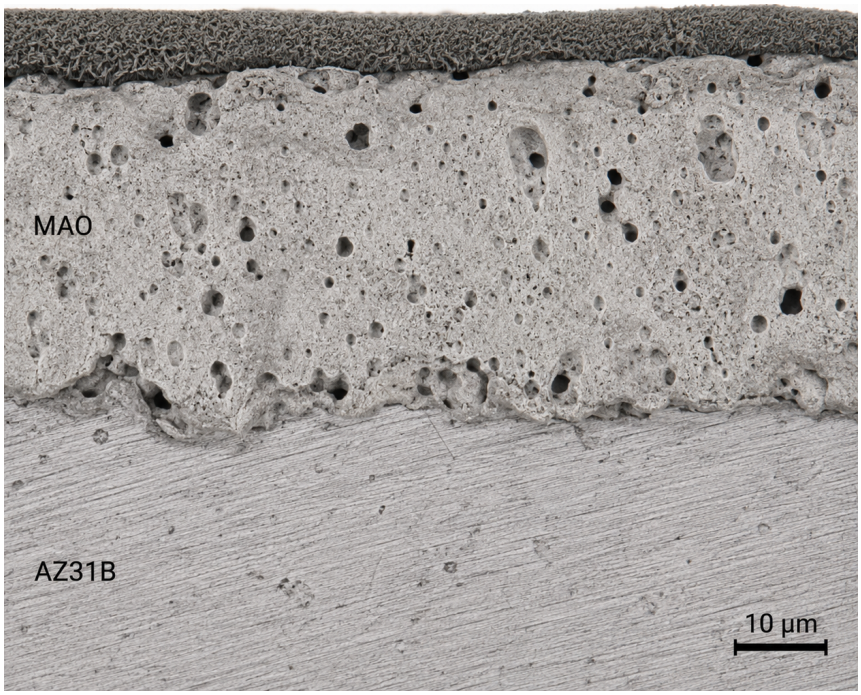

Figure 4: Coating cross-section.

3.2 Response of polarization in chloride and acidic sulfate solutions

Based on the data provided in Table 1, it can be seen that the corrosion current density gradually reduces from AZ31B to AMAO and then to AMAO@P-ZPNF. In the case of 3.5 wt% NaCl solution, the polarization test on AZ31B revealed that $E_{corr} = -1.472$ V and $i_{corr} = 4.862 \times 10^{-5}$ A cm^{-2}. The changes in values after the micro-arc oxidation process include the shift of E_{corr} to -1.414 V and a significant reduction in i_{corr} down to 1.478×10^{-6} A cm^{-2}, confirming that the coating prevents active corrosion process in the chloride solution. The highest value of polarization is observed for the AMAO@P-ZPNF coating, which shows a value of E_{corr} equal to -1.132 V and $i_{corr} = 3.775 \times 10^{-8}$ A cm^{-2}.

Table 1: Polarization values in chloride and acidic sulfate solutions.

Surface	3.5 wt% NaCl		0.5 mol L^{-1} H_2SO_4	
	E_{corr} (V)	i_{corr} (A cm^{-2})	E_{corr} (V)	i_{corr} (A cm^{-2})
AZ31B	-1.472	4.862×10^{-5}	-1.592	2.747×10^{-4}
AMAO	-1.414	1.478×10^{-6}	-1.511	8.029×10^{-6}
AMAO@P-ZPNF	-1.132	3.775×10^{-8}	-1.335	9.497×10^{-8}

From the chloride polarization diagrams of Figure 5, it can be seen how the transition happens from the active AZ31B corrosion mode to that of the low current AMAO@P-ZPNF. From the diagram it can also be observed that the minimum of the AMAO@P-ZPNF graph occurs at a more positive potential compared to the other two surfaces, as well as having a lower value for i_{corr}. Thus, the effect of the decreased value of i_{corr} is more significant than just a minor change in mixed potential.

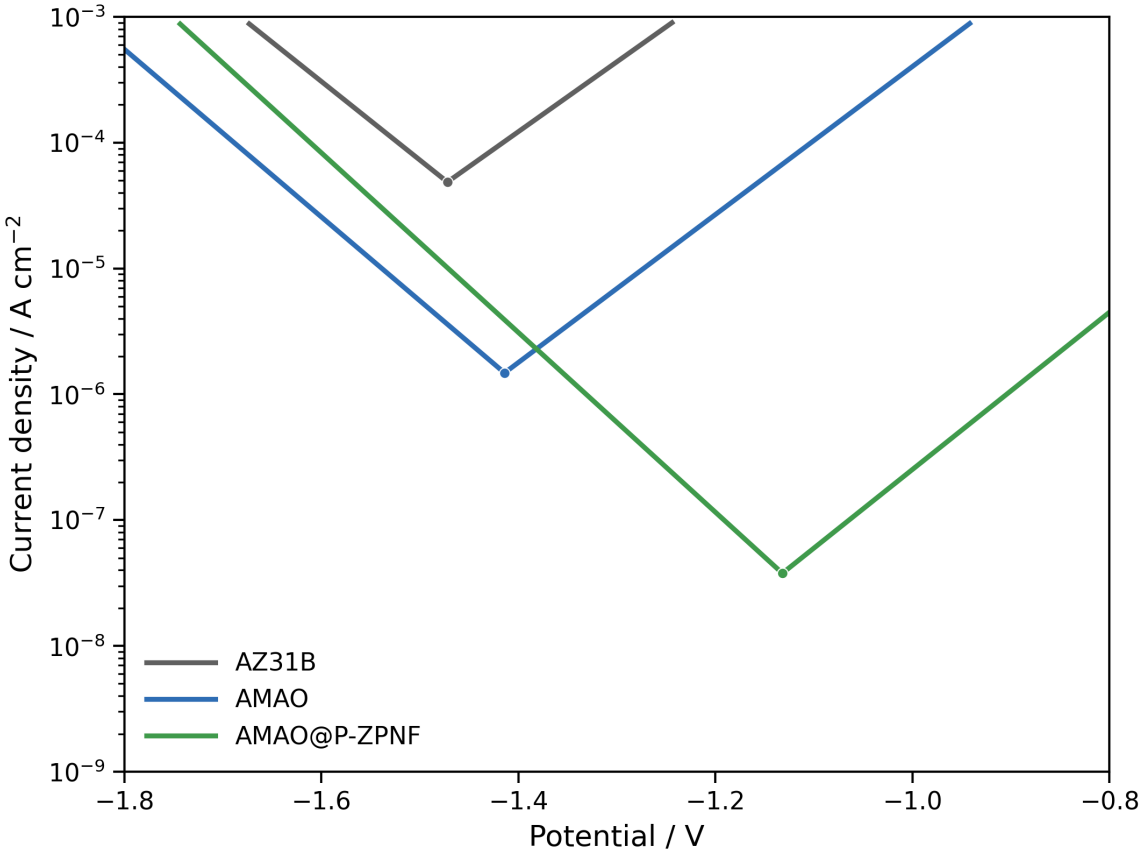

Figure 5: Polarization in NaCl.

The current density increases when an acidic sulfate solution is used, and there is no coating on the AZ31B. The rise from 4.862×10^{-5} A cm^{-2} in NaCl solution to 2.747×10^{-4} A cm^{-2} in the H_2SO_4 solution indicates a factor of 5.65 times more current. As seen from the plots in Figure 6, the AMAO provides protection; however, the highest suppression is obtained with the AMAO@P-ZPNF coating. The final coating lowers i_{corr} to 9.497×10^{-8} A cm^{-2}, which is approximately 2893 times lower than the uncoated alloy in the same acidic medium.

Trends in efficiency of current reduction are also observed similarly. In NaCl, AMAO decreases i_{corr} by 96.96%, while AMAO@P-ZPNF reduces it by 99.92%. The difference between these two treatments is much bigger for the acid case, where i_{corr} decreases by 97.08% with AMAO and 99.97% with AMAO@P-ZPNF. It can be clearly seen on the graph (Figure 7),

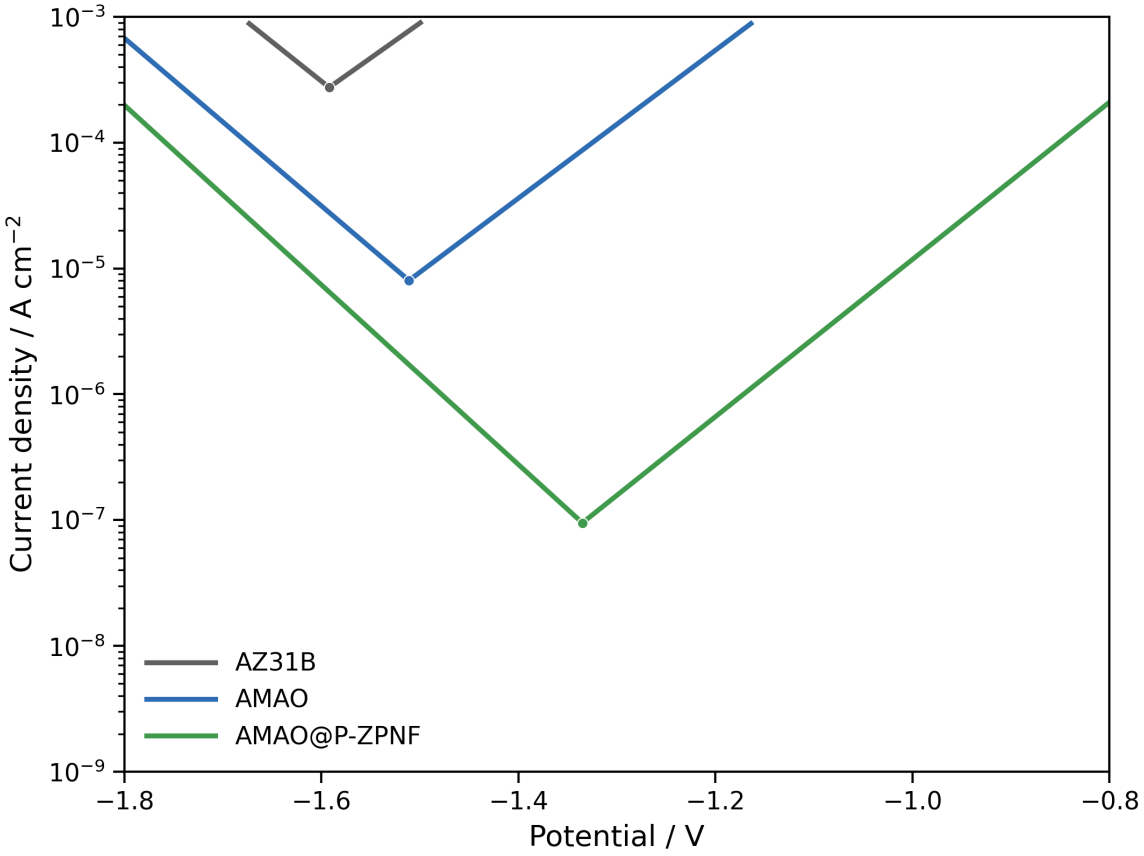

Figure 6: Polarization in acidic sulfate.

which shows the decrease in current density due to the nanoflower treatment. AMAO greatly improves the properties of the AZ31B surface, yet, it still leaves an almost 40-fold (for NaCl) or 85-fold (for acid) greater current density compared to AMAO@P-ZPNF.

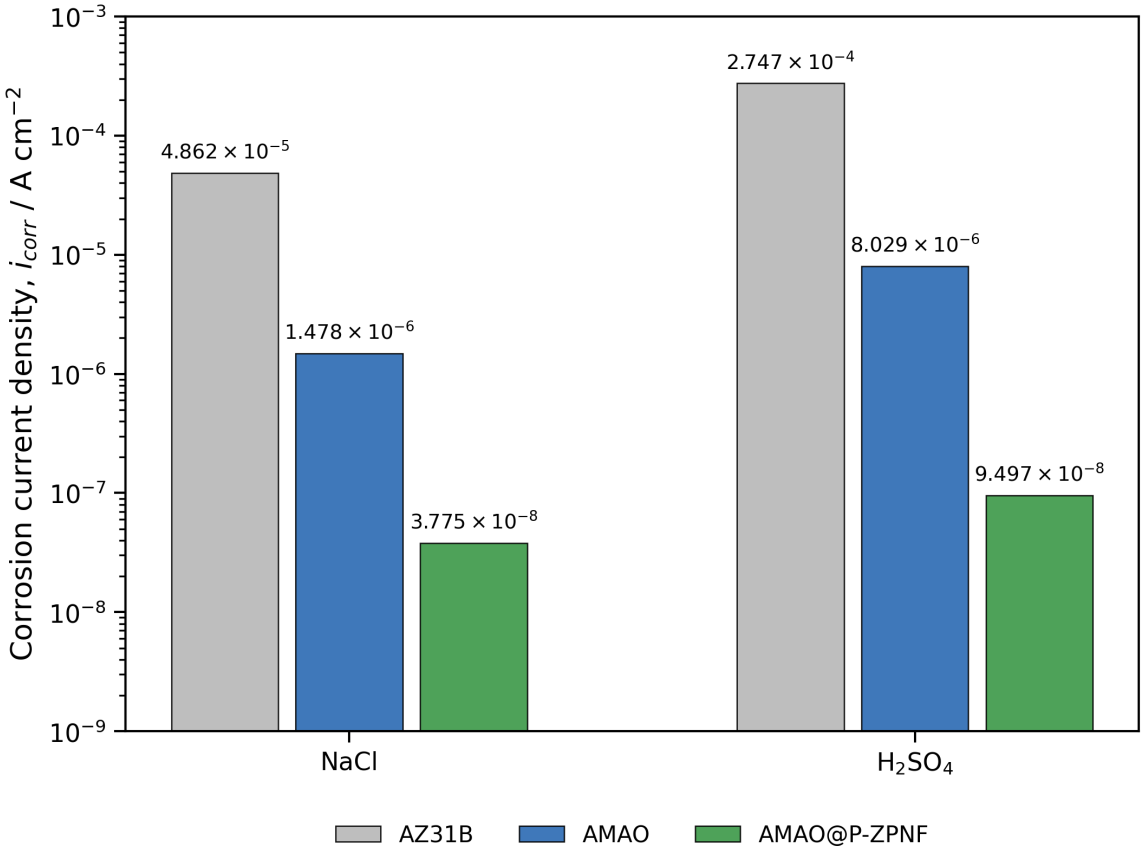

Figure 7: Corrosion current density.

This result suggests that not just the mixed potential is altered in the corrosion process when the modified coating is applied but rather that the mechanism of corrosion is altered. The shift towards a positive direction of E_{corr} is combined with a multi-order reduction of i_{corr} demonstrating that both parameters are altered. Both effects are achieved thanks to the hydrophobic nature of the outer zinc phosphate layer and separation of the electrolyte from the surface by the MAO layer. This result is especially apparent in case of acidic sulfate solution where AZ31B demonstrates high corrosion rate while AMAO@P-ZPNF maintains extremely low current density.

3.3 Impedance response and resistance enhancement

Impedance values shown in Table 2 can explain the above-mentioned polarisation response of unmodified AZ31B. Both in chloride solution and in acid, uncoated AZ31B presents low resistance (R_c) and charge transfer resistance (R_{ct}). In case of NaCl solution, these parameters are 89.3 Ω cm^2 and 75.89 Ω cm^2 respectively. In case of acidic solution, both values fall down to 32.55 and 33.81 Ω cm^2 correspondingly. The low values show that the native film has poor barrier resistance and that charge transfer at active regions is not strongly hindered.

Table 2: Coating and charge-transfer resistances.

Surface	3.5 wt% NaCl		0.5 mol L^{-1} H_2SO_4	
	R_c (Ω cm^2)	R_{ct} (Ω cm^2)	R_c (Ω cm^2)	R_{ct} (Ω cm^2)
AZ31B	8.93×10^1	7.589×10^1	3.255×10^1	3.381×10^1
AMAO	3.989×10^3	1.479×10^4	2.108×10^3	7.169×10^3
AMAO@P-ZPNF	8.759×10^5	3.517×10^6	6.293×10^5	2.534×10^6

In the case of micro-arc oxidation, the enhancement factor of R_c is increased from 89.3 to 3.989×10^3 Ω cm^2 for NaCl and from 32.55 to 2.108×10^3 Ω cm^2 for acid. As shown in Figure 8, the coating-resistance evaluation suggests that, compared to AMAO, AMAO@P-ZPNF results in much higher R_c, namely 8.759×10^5 Ω cm^2 and 6.293×10^5 Ω cm^2 in NaCl and H_2SO_4, respectively. Clearly, such values of coating resistance indicate a significant reduction in the electrolyte transportation through the coating.

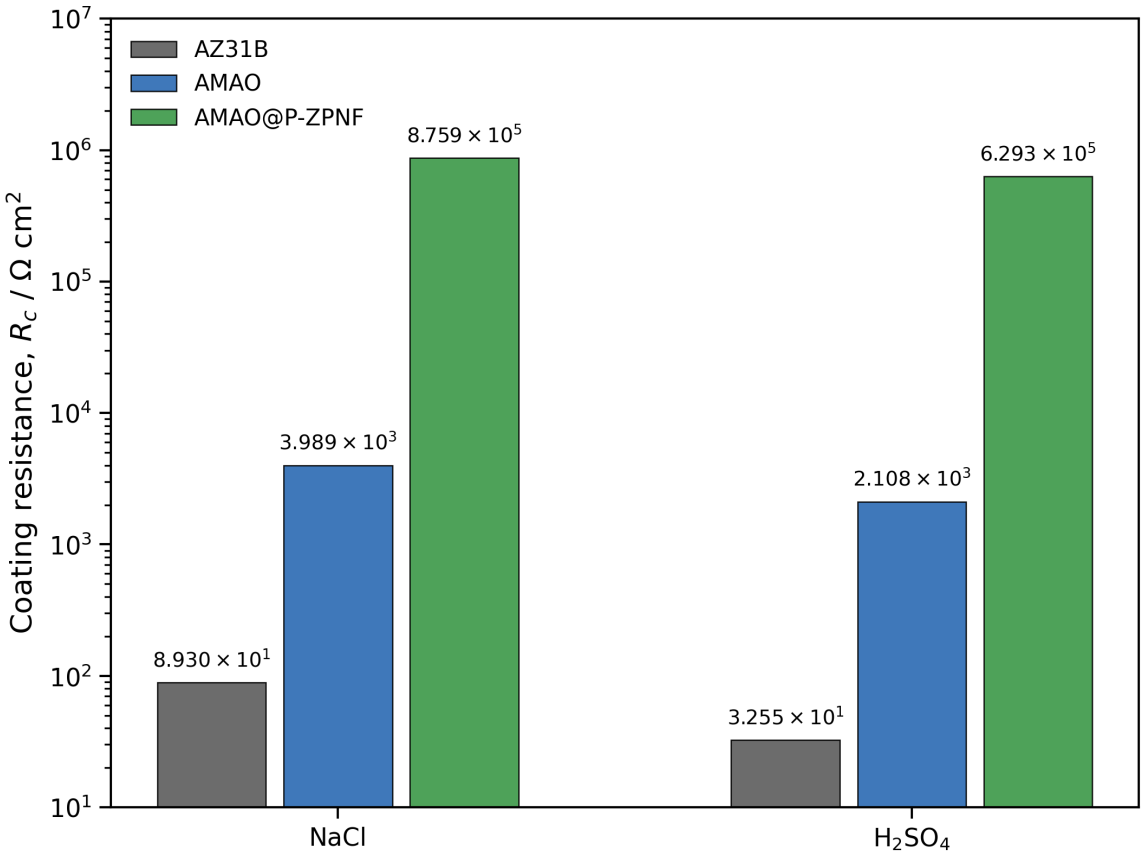

Figure 8: Coating resistance.

Charge-transfer resistance shows the similar hierarchy but with a higher discrimination level between surface states. The application of AMAO leads to the enhancement of R_{ct} value to 1.479×10^4 Ω cm^2 for NaCl solution and to 7.169×10^3

Ω cm^2 in the case of acid. The amplification factors of charge-transfer resistance for those cases will be equal to 1.949×10^2 and 2.120×10^2 correspondingly. According to the data from the figure below, the interfacial barrier is considerably higher in the case of the composite sample with a value of 3.517×10^6 Ω cm^2 in NaCl solution and 2.534×10^6 Ω cm^2 in an acidic environment

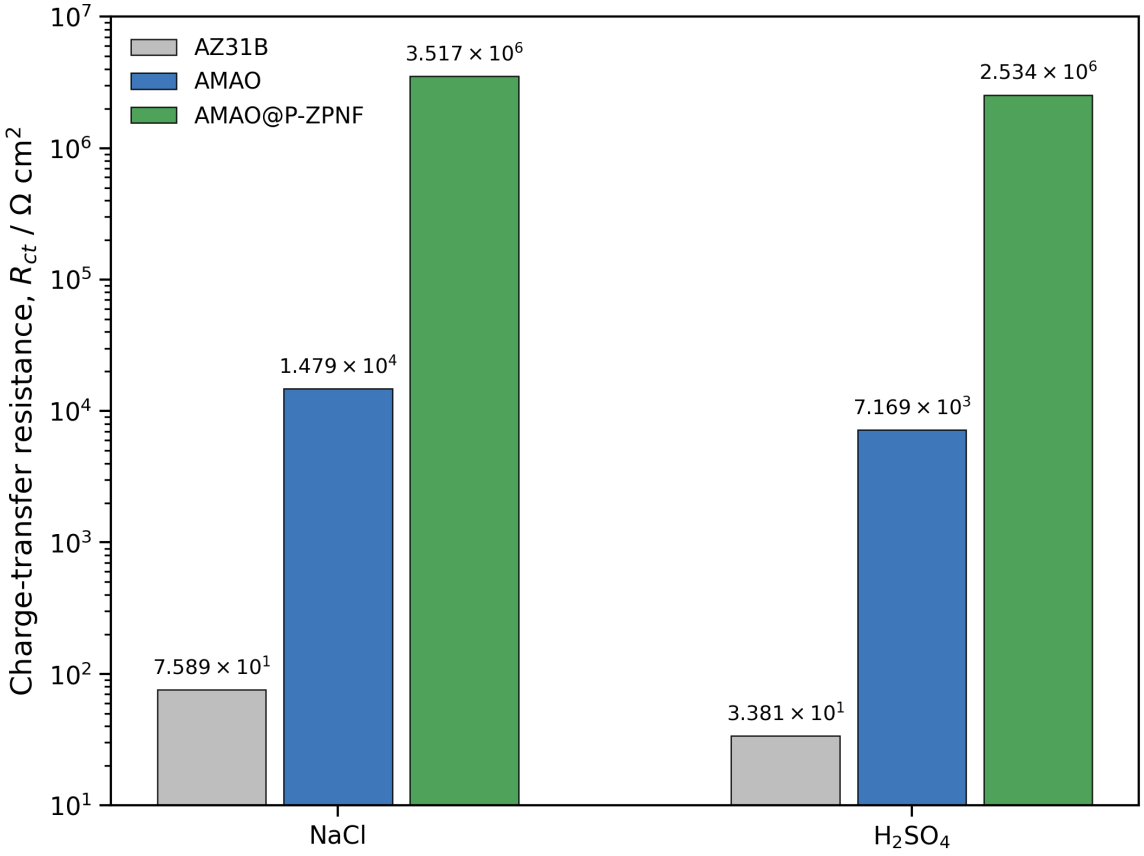

Figure 9: Charge-transfer resistance.

The difference between the resistance of R_c and R_{ct} explains the superior performance of AMAO@P-ZPNF compared to AMAO. If the coating has a high value for R_c, but not for R_{ct}, it can eventually be compromised if the electrolytes reach the reactive centers. Alternatively, having a large value of R_{ct} but little R_c means that the coating may be permeable, slowing down the interfacial reaction temporarily but not preventing it. Both of these factors do not apply to AMAO@P-ZPNF since both resistances have been improved by many orders of magnitude. The presence of zinc phosphate nanoflowers impedes the flow of electrolyte in the coating, while the MAO-assisted interface exhibits a high level of protection against Faradaic corrosion reaction.

3.4 Barrier effect and acid trapping

As can be seen from the numerical data provided in Table 3, there are significant electrochemical effects associated with the presence of two anti-corrosive coatings. For uncoated AZ31B, $\Phi = 1$. For AMAO, $\Phi = 82.58$. Finally, for the combination of coatings, $\Phi = 1.067 \times 10^4$. It is shown that both current reduction and charge-transfer resistance enhancement take place in both electrolytes.

Table 3: Current reduction, charge-transfer resistance amplification, and barrier score.

Surface	η_i NaCl (%)	η_i H_2SO_4 (%)	$A_{R_{ct}}$ NaCl	$A_{R_{ct}}$ H_2SO_4	Φ
AZ31B	0	0	1	1	1
AMAO	96.96	97.08	1.949×10^2	2.120×10^2	82.58
AMAO@P-ZPNF	99.92	99.97	4.634×10^4	7.495×10^4	1.067×10^4

For AMAO and AMAO@P-ZPNF, the respective acid-retention factors are 1.09 and 1.62. From the AMAO value just above unity, we can conclude that the oxide coating retains a relatively similar degree of advantage in acid conditions over AZ31B without any coating, even though the absolute resistance values in H_2SO_4 are lower. However, the AMAO@P-ZPNF value is higher at 1.62, reflecting greater relative advantages in terms of charge transfer resistance under acid corrosion

conditions. This comparison is plotted together in Figure 10, where we observe that the highest barrier score corresponds to the greatest acid retention ability.

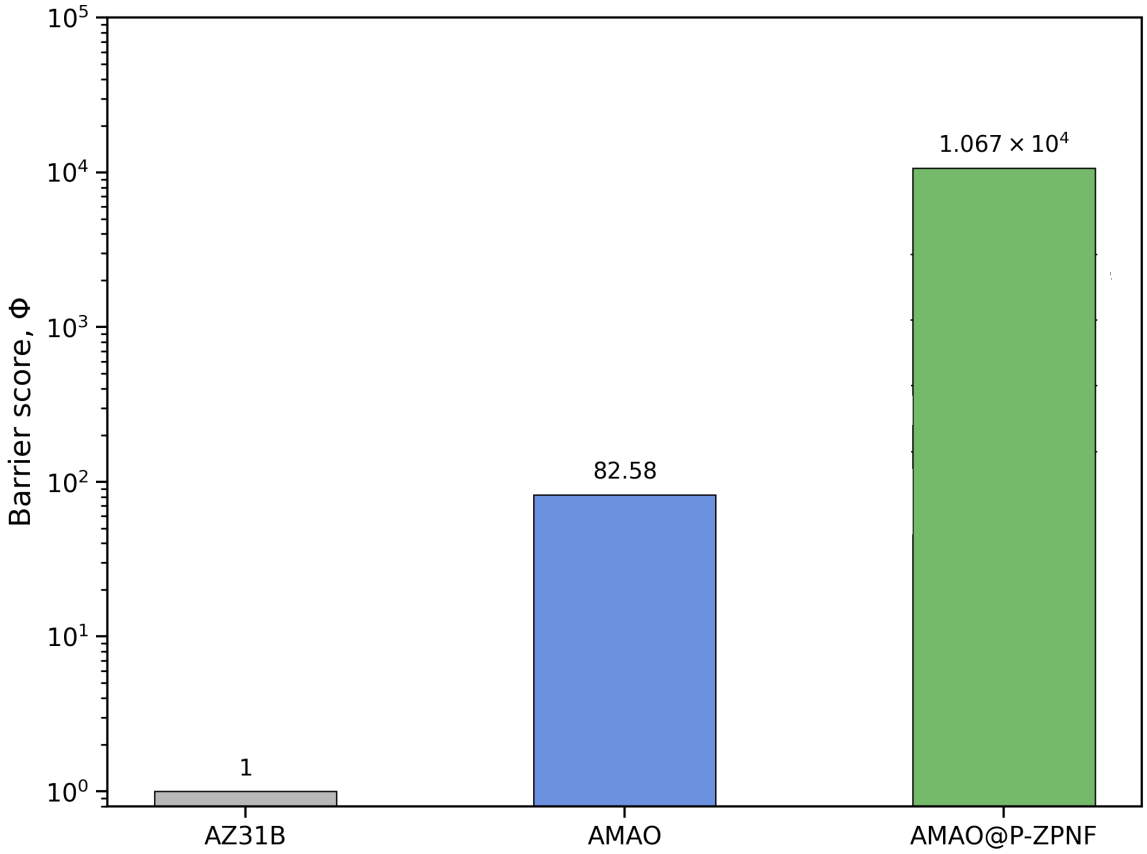

Figure 10: Barrier score and acid retention.

The high value of Φ in the case of AMAO@P-ZPNF cannot be attributed to one electrochemical characteristic. This film demonstrates a low corrosion current density, a high film resistance, a high charge transfer resistance, and high acid retention capability among the three materials. From the numerical analysis, a coupled mechanism is observed whereby electrolyte migration is prevented prior to the electrolyte reaching the internal oxide layer, while charge transfer continues to be highly restricted.

3.5 Chloride corrosion path

Corrosion of AZ31B occurs via magnesium dissolution and hydrogen evolution. Chloride ion destabilizes magnesium hydroxide and accelerates magnesium chloride formation, thus allowing active sites to react again. It, therefore, implies that there is localized corrosion in the uncoated alloy. The results presented ($i_{\text{corr}} = 4.862 \times 10^{-5}$ A cm^{-2} and $R_{ct} = 75.89$ Ω cm^2) illustrate weak charge transfer restriction.

For AMAO, the oxide film prevents the solution from contacting with the substrate directly. As evidenced by the decreased corrosion current of 1.478×10^{-6} A cm^{-2}, such film reduces the electrochemical oxidation of the substrate. The increased resistance of $R_c = 3.989 \times 10^3$ Ω cm^2 and $R_{ct} = 1.479 \times 10^4$ Ω cm^2 indicates both slower electrolyte transportation and electrochemical reaction rate. While no other weaknesses of the coating have been observed, some evidence exists in the porous discharge morphology in Figure 2 and the discharge structure in the cross-section in Figure 4.

In comparison, for the AMAO@P-ZPNF coating, the chloride diffusion path becomes much harder. Due to the hydrophobic surface covered with nanoflowers illustrated in Figure 3, the diffusion length and tortuosity are increased. Also, part of the pores within the discharge structure would be sealed. Therefore, ionic continuity would not be achieved easily by the chloride solution inside the coating. Hence, we see decreased corrosion current of $i_{\text{corr}} = 3.775 \times 10^{-8}$ A cm^{-2} and resistance increase of $R_{ct} = 3.517 \times 10^6$ Ω cm^2. The corrosion protection mechanism for the new material involves both limited chloride penetration and reduced electrochemical activity at the inner surface.

3.6 Acidic sulfate corrosion mechanism

As expected, the acid promotes corrosion through solvation of the oxide/hydroxide films. In the case of AZ31B Mg alloy without coating, the corrosion current density is as high as 2.747×10^{-4} A cm^{-2}, and the values of resistances R_c and R_{ct}

are decreased to 32.55 Ω cm^2 and 33.81 Ω cm^2.

Even after MAO application, the alloy shows high activity in the H_2SO_4 solution, where its corrosion current density is decreased to 8.029×10^{-6} A cm^{-2}. However, its $R_c = 2.108 \times 10^3$ Ω cm^2 and $R_{ct} = 7.169 \times 10^3$ Ω cm^2 prove the protection from corrosion due to the presence of the passive film. The reduction of acid values in comparison with NaCl indicates the high susceptibility of the MAO film to acidic corrosion.

AMAO@P-ZPNF exhibits a considerable acid resistance capacity. In acid, the i_{corr} value for the film is 9.497×10^{-8} A cm^{-2}, which is only 2893 times smaller than the AZ31B bare metal sample's. Its R_c and R_{ct} parameters range from 10^5 to 10^6 Ω cm^2. It becomes hard for acid to interact with electroactive magnesium centers through the nanoflowers film due to limited liquid penetration before MAO film starts decaying. Chemical stability of the phosphate film prevents interaction with the magnesium substrate; hydrophobicity decreases acid wetting.

The comparison of NaCl and H_2SO_4 solutions shows the need for two-electrolyte evaluation. While a coating can protect very effectively against the penetration of chloride solution, the oxide will dissolve in the presence of acid. It is possible that an acidic solution may also infiltrate the coating through the defects in order to cause corrosion. The acid retention ratio proves the superior performance of the coating in acid rather than in chloride solution.

3.7 Integration of protection mechanism

This combination of responses indicates an overall multi-layered mechanism of protection. The MAO coating gives a solid oxide basis on the one hand and protects the substrate from direct exposure to the solution, while the nanoflowers block access of pores, increase roughness, and form an additional phosphate layer. Hydrophobization increases the distance between the metal and the liquid and maintains trapped air in the roughness regions.The combined actions described above have effects that decrease ion transport as well as reaction kinetics at the interface.

This phenomenon is illustrated by increasing both R_c and R_{ct}. Increasing R_c suggests better physical blocking, but no necessarily long-term stability of the interface. Conversely, increased R_{ct} suggests slower electrochemical reactions, but does not guarantee that electrolyte permeability will be sufficiently low. Both parameters increase by several orders of magnitude in the case of AMAO@P-ZPNF. Corrosion current density stays relatively low due to low transport of chloride and acid ions and unresponsive charge transfer at the interface.

The maximum barrier score is provided by AMAO@P-ZPNF as the coating does not rely on any single method of protection. While barrier score is 1 for AZ31B, it becomes 82.58 for AMAO and 1.067×10^4 for AMAO@P-ZPNF, as seen in Figure 10. These changes represent the combined effect of suppressing currents in both electrolytes and increasing charge transfer resistance in both electrolytes. The coating thus represents a more comprehensive protection status than just MAO treatment alone.

The above analysis is consistent with the observations of the surface morphology. Discharge pores present in AMAO may hold the electrolyte inside and become potential corrosion paths. Zinc phosphate nanoflowers coat the oxide surface and hinder this effect. Finally, the hydrophobic layer decreases the ability of chloride or acid solutions to remain stably adsorbed at the surface. This leads to a smaller effective surface, larger diffusion path, and decreased charge transfer reaction rates.

4. Conclusions

From the results obtained for the electrochemical protection of AZ31B magnesium alloy, it can be noted that it progressively improves when going from uncoated AZ31B to AMAO and further to AMAO@P-ZPNF in both 3.5 wt% NaCl and 0.5 mol L^{-1} H_2SO_4 solutions. Uncoated AZ31B demonstrates rapid corrosion, having i_{corr} equal to 4.862×10^{-5} A cm^{-2} and 2.747×10^{-4} A cm^{-2} in NaCl and acid, respectively. Its relatively low values of R_c and R_{ct} prove that the native oxide film cannot afford stable electrochemical protection in either electrolyte.

Micro-arc oxidation provides an evident protective oxide layer. For AMAO in NaCl, the current density of corrosion decreases to 1.478×10^{-6} A cm^{-2}, resulting in a current-reduction efficiency of 96.96%. For the same coating in acid, $i_{corr} = 8.029 \times 10^{-6}$ A cm^{-2} (97.08%). Its charge-transfer resistance increases to 1.479×10^4 Ω cm^2 in NaCl and 7.169×10^3 Ω cm^2 in acid. Thus, we can state that MAO is indeed a suitable method of oxide formation despite the presence of the discharge pores and microcracks.

The response for the AMAO@P-ZPNF coating proves to be the highest among all three cases. For the mentioned coating, the corrosion current density equals 3.775×10^{-8} A cm^{-2} and 9.497×10^{-8} A cm^{-2} in NaCl and acid, respectively, providing current-reduction efficiencies of 99.92% and 99.97%. For the same case, charge-transfer resistance grows to 3.517×10^6 Ω cm^2 in NaCl and 2.534×10^6 Ω cm^2 in acid. The coating resistances remain high for both electrolyte types with $R_c = 8.759 \times 10^5$ Ω cm^2 in NaCl and 6.293×10^5 Ω cm^2 in acid.

The barrier scores are increased from 1 for AZ31B to 82.58 for AMAO and 1.067×10^4 for AMAO@P-ZPNF. The acid-retention value for AMAO@P-ZPNF is 1.62. It indicates significant relative protection of AMAO@P-ZPNF against corrosion under acidic sulfate conditions. The enhanced protection of this sample was due to the combined contribution of the MAO oxide coating, zinc phosphate sealing, exclusion of hydrophobic liquid phases, long diffusion pathways, and inhibited charge-transfer reaction at interfaces. Consequently, AMAO@P-ZPNF proved to be the best of the three investigated AZ31B coating systems in both chloride and acidic sulfate environments.

Conflict of interest

The author declares no conflict of interest.

References

[1] Song, G. L., & Atrens, A. (1999). Corrosion mechanisms of magnesium alloys. Advanced engineering materials, 1(1), 11-33.
[2] Atrens, A., Song, G. L., Liu, M., Shi, Z., Cao, F., & Dargusch, M. S. (2015). Review of recent developments in the field of magnesium corrosion. Advanced Engineering Materials, 17(4), 400-453.
[3] ZHANG, J., HUANG, W. J., Dietzel, W., Kainer, K. U., Blawert, C., & KE, W. (2006). Review of studies on corrosion of magnesium alloys. Transactions of Nonferrous Metals Society of China, 16, s763-s771.
[4] Song, G. (2007). Control of biodegradation of biocompatable magnesium alloys. Corrosion science, 49(4), 1696-1701.
[5] Gray, J., & Luan, B. (2002). Protective coatings on magnesium and its alloys—a critical review. Journal of alloys and compounds, 336(1-2), 88-113.
[6] Chen, X. B., Birbilis, N., & Abbott, T. B. (2011). Review of corrosion-resistant conversion coatings for magnesium and its alloys. Corrosion, 67(3), 035005-1.
[7] Hornberger, H., Virtanen, S., & Boccaccini, A. R. (2012). Biomedical coatings on magnesium alloys–a review. Acta biomaterialia, 8(7), 2442-2455.
[8] Yerokhin, A. L., Nie, X., Leyland, A., Matthews, A., & Dowey, S. J. (1999). Plasma electrolysis for surface engineering. Surface and coatings technology, 122(2-3), 73-93.
[9] Guo, H. F., An, M. Z., Huo, H. B., Xu, S., & Wu, L. J. (2006). Microstructure characteristic of ceramic coatings fabricated on magnesium alloys by micro-arc oxidation in alkaline silicate solutions. Applied surface science, 252(22), 7911-7916.
[10] Arrabal, R., Matykina, E., Viejo, F., Skeldon, P., & Thompson, G. E. (2008). Corrosion resistance of WE43 and AZ91D magnesium alloys with phosphate PEO coatings. Corrosion Science, 50(6), 1744-1752.
[11] Walsh, F. C., Low, C. T. J., Wood, R. J. K., Stevens, K. T., Archer, J., Poeton, A. R., & Ryder, A. (2009). Plasma electrolytic oxidation (PEO) for production of anodised coatings on lightweight metal (Al, Mg, Ti) alloys. Transactions of the IMF, 87(3), 122-135.
[12] Wenzel, R. N. (1936). Resistance of solid surfaces to wetting by water. Industrial & engineering chemistry, 28(8), 988-994.
[13] Cassie, A. B. D., & Baxter, S. (1944). Wettability of porous surfaces. Transactions of the Faraday society, 40, 546-551.
[14] Quéré, D. (2008). Wetting and roughness. Annu. Rev. Mater. Res., 38, 71-99.
[15] Ou, J., Hu, W., Xue, M., Wang, F., & Li, W. (2013). Superhydrophobic surfaces on light alloy substrates fabricated by a versatile process and their corrosion protection. ACS applied materials & interfaces, 5(8), 3101-3107.
[16] Cui, L. Y., Liu, H. P., Zhang, W. L., Han, Z. Z., Deng, M. X., Zeng, R. C., ... & Wang, Z. L. (2017). Corrosion resistance of a superhydrophobic micro-arc oxidation coating on Mg-4Li-1Ca alloy. Journal of Materials Science & Technology, 33(11), 1263-1271.
[17] Ran, M., Zheng, W., & Wang, H. (2019). Fabrication of superhydrophobic surfaces for corrosion protection: A review. Materials Science and Technology, 35(3), 313-326.
[18] Biallozor, S., & Kupniewska, A. (2005). Conducting polymers electrodeposited on active metals. Synthetic Metals, 155(3), 443-449.
[19] Van Ooij, W. J., Zhu, D., Stacy, M., Seth, A., Mugada, T., Gandhi, J., & Puomi, P. J. T. S. (2005). Corrosion protection properties of organofunctional silanes—an overview. Tsinghua Science and technology, 10(6), 639-664.
[20] Zhang, J., Gu, C., & Tu, J. (2017). Robust slippery coating with superior corrosion resistance and anti-icing performance for AZ31B Mg alloy protection. ACS applied materials & interfaces, 9(12), 11247-11257.
[21] Stern, M., & Geary, A. L. (1957). Electrochemical polarization: I. A theoretical analysis of the shape of polarization curves. Journal of the electrochemical society, 104(1), 56-63.
[22] Mansfeld, F. (1990). Electrochemical impedance spectroscopy (EIS) as a new tool for investigating methods of corrosion protection. Electrochimica Acta, 35(10), 1533-1544.
[23] Macdonald, J. R. (1992). Impedance Spectroscopy‖ Annals of Biomedical Engineering.
[24] Lazanas, A. C., & Prodromidis, M. I. (2023). Electrochemical impedance spectroscopy—a tutorial. *ACS Measurement Science Au*, 3(3), 162–193.
[25] Yang, C., Wang, C., Zhao, X., Shen, Z., Wen, M., Zhao, C., ... & Zeng, X. (2024). Superhydrophobic surface on MAO-processed AZ31B alloy with zinc phosphate nanoflower arrays for excellent corrosion resistance in salt and acidic environments. Materials & Design, 239, 112769.